

Salicylideneanilines-Based Covalent Organic Frameworks as Chemoselective Molecular Sieves

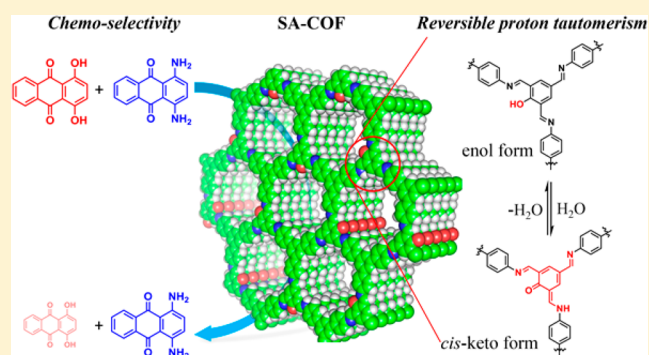
Guo-Hong Ning,[†] Zixuan Chen,[†] Qiang Gao,[†] Wei Tang,[‡] Zhongxin Chen,[†] Cuibo Liu,[†] Bingbing Tian,[†] Xing Li,[†] and Kian Ping Loh^{*,†}

[†]Department of Chemistry, National University of Singapore, 3 Science Drive 3, Singapore 117543, Singapore

[‡]Institute of Materials Research and Engineering, A*STAR, 2 Fusionopolis Way, Innovis, Singapore 138634, Singapore

Supporting Information

ABSTRACT: Porous materials such as covalent organic frameworks (COFs) are good candidates for molecular sieves due to the chemical diversity of their building blocks, which allows fine-tuning of their chemical and physical properties by design. Tailored synthesis of inherently functional building blocks can generate framework materials with chemoresponsivity, leading to controllable functionalities such as switchable sorption and separation. Herein, we demonstrate a chemoselective, salicylideneanilines-based COF (SA-COF), which undergoes solvent-triggered tautomeric switching. This is unique compared to solid-state salicylideneanilines' counterpart, which typically requires high energy input such as photo or thermal activation to trigger the enol–keto tautomerism and *cis*–*trans* isomerization. Accompanying the tautomerization, the ionic properties of the COF can be tuned reversibly, thus forming the basis of size-exclusion, selective ionic binding or chemoseparation in SA-COF demonstrated in this work.



INTRODUCTION

Covalent organic frameworks (COFs) are a class of crystalline porous polymer that allows atomically precise integration of functionalities into an extended, porous network.^{1–5} Although COFs have great application potentials in wide ranging fields including gas storage,^{6,7} energy storage,^{8–10} drug delivery,¹¹ catalysis,^{12–14} and electronic application,^{15–17} molecular separation on the basis of size, charge, and functionality by using COFs' ordered pores and channels is not widely reported. One challenge is the difficulty in tailoring the interactions between pore surface and sorbents. Wang's group used presynthetic modification to prepare the thioether-functionalized COF-LZU8 for sensing and removal of mercury(II) ions.¹⁸ Jiang's group improved CO₂ adsorption by postsynthetic modification of COFs' pore surface with various functional groups.⁷ Incorporating inborn functionalities into the pores that can interact with molecules based on noncovalent interactions is attractive due to the ability to engender a chemoresponsive response to the environment. One strategy is to construct the COF from monomers that can undergo dynamic structural changes via coordination or noncovalent interactions, i.e., protonation-induced tautomerization or *cis*–*trans* isomerization. Triggered by environmental cues (solvent and pH), dramatic changes in the acidic character or ionicity of the functional groups occur following tautomerization and *cis*–*trans* isomerization, thus imparting inborn selectivity to targeted molecules in the pores. In actuality, the properties of the porous framework structure are

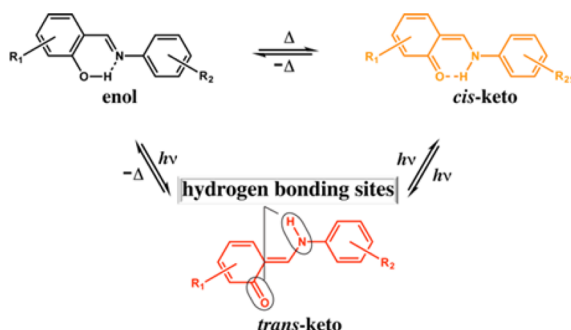
often different from the building blocks due to the cross-linking and tight packing of the molecular layers. The rigidity of the COF framework can also restrict the rotational or flexural motions of the building blocks. Thus far, there are no reports of reticular synthesis of a COF, which can undergo solvent-triggered tautomerization.

Salicylideneanilines (SA), a class of Schiff bases comprising salicylaldehyde and aniline derivatives, have attracted great attention due to their unique photo- and thermochromic properties in the solid state, which can find applications in sensors, optical data storage, and display devices.^{19–22} The mechanism of reversible color change of SA in response to external simulation (i.e., temperature and light) in the solid state is well studied and suggests a tautomeric structural transformation promoted by proton transfer.^{23–25} First, an equilibrium exists between the white-colored enol form at lower temperature and the yellow-colored *cis*-keto form at room temperature (rt), and in both forms, a cyclic intermediate stabilized by intramolecular hydrogen bonding is observed (Scheme 1). Second, the isomerization between the *cis*-keto and the red-colored *trans*-keto form can be induced by light.^{23,24} The resulting *trans*-keto form relaxes back to the *cis*-keto form via thermo- or photoisomerization (Scheme 1).²⁵ Accompanying the reversible color change of SA, the hydrogen and ionic bonding properties of SA change dramatically during

Received: March 17, 2017

Published: June 15, 2017

Scheme 1. Reversible Proton Tautomerism of Salicylideneanilines under Thermo- and Photochromism Pathways^a



^aThe *trans*-keto form bears two accessible hydrogen-bonding sites.

the proton tautomerism (slightly acidic in the enol form and basic in the *cis*- and *trans*-keto form) (Scheme 1).

The reversible switching of functionality in SA motivated us to consider integrating SA moieties into COFs to make SA-COF. Interestingly, SA-COF exhibits reversible proton tautomerism triggered by adsorption and desorption of water molecules (Figure 1). This is the first report that the transformation between the *cis*- and *trans*-keto form in the solid state can be initiated by low-energy input, i.e., solvent, instead of high-energy input, i.e., photoirradiation. Importantly, the tautomerization allows a dynamic change in the ionic properties of the pores in response to chemical cues, thus forming the basis of size-exclusion or selective ionic binding. The tunable functionality of the pore surface allows SA-COF to bind to positively charged molecules in basic conditions, while excluding it in acidic conditions. More interestingly, SA-COF selectively binds molecules with aromatic hydroxyl groups over aromatic amino groups following conversion to the *trans*-keto stage (Scheme 1).

EXPERIMENTAL SECTION

Synthesis of SA-COF. 2,4,6-Triformylphenol (TFP) (14.3 mg, 0.80 mmol), 1,3,5-tris(4-aminophenyl)benzene (TAB) (27.5 mg, 0.80 mmol), 0.5 mL of *n*-butanol, 0.5 mL of 1,2-dichlorobenzene, and 0.1 mL of 6 M aqueous acetic acid were added into a 10 mL Schlenk storage tube (Synthware, o.d. 28 × L 80 mm, high-vacuum valve size 0–8 mm, with PTFE O-ring, wiper).²⁶ This mixture was sonicated for 15 min in order to get a homogeneous dispersion. The tube was then flash frozen at 77 K (liquid N₂ bath) and degassed with three freeze–pump–thaw cycles, and then the tube was sealed and heated at 120 °C for 7 days. A dark red colored precipitate produced was collected by decantation and washed, and solvent exchanged with anhydrous tetrahydrofuran (10 mL) several times. The resultant products were dried at 120 °C under vacuum overnight to give a light yellow colored powder in 81% (30 mg) isolated yield. FT-IR (KBr, cm⁻¹): 2955 (w), 2925 (w), 2863 (w), 1631 (s, C=O), 1582 (s, C=N), 1501 (s, C=C in enamine), 1451 (s, aromatic C=C), 1141 (s), 829 (s). Anal. Calcd for C₉₉O₃H₆₃N₉: C, 83.35; H, 4.45; N, 8.84. Found: C, 80.55; H, 5.05; N, 8.04.

Selective Dye Separation Experiment. All the batch adsorption experiments were conducted at rt in the dark. Initial dye concentrations were fixed to be 50 μM. Typically 5 mg of SA-COF was added into 5 mL of dye solution, and the mixture was sonicated for 10 s to get a well-dispersed solution and then stirred at rt on a hot plate at 700 rpm. At appropriate time intervals, the mixture was filtered in syringes equipped with Whatman 0.45 μm membrane filters. The concentration of dye in the filtrate was detected using an ultraviolet–visible spectrometer (Shimadzu UV-2600) at a wavelength of

maximum absorbance (665, 608, and 664 nm for methylene blue (MB) in neutral, basic, and acidic conditions, respectively; 413 nm for anthraflavic acid (AA) in basic conditions; 419 nm for Chrome azurol S (CA); 550 nm for rhodamine B (RB); 590 nm for 1,4-diaminoanthraquinone (DAQ), and 546 nm for 1,4-dihydroxyanthraquinone (DHQ)). The removal efficiency of dye was calculated as follows:

$$\text{Removal efficiency (\%)} = (C_0 - C_t)/C_0 \times 100 \quad (1)$$

where C₀ and C_t are the concentration of dyes at initial condition and in the filtrate, respectively.

For the molecular separation study, 5 mg of SA-COF was suspended in 5 mL of water solution (pH = 12) for 5 min and then passed through a Whatman (0.45 μm) membrane filter to give an SA-COF-equipped filter. The resulting SA-COF-equipped filter was washed with 5 mL of water solution (pH = 12) once before using it for the separation experiments without any further processing.

HPLC was performed with an Agilent 1200 HPLC equipped with a diode-array ultraviolet detector and a Phenomenex Luna C18 (2) column (2.0 × 150 mm, 5 μm particle size). The sample injection volume was 20 μL, and the flow rate was 0.7 mL min⁻¹. The mobile phase for HPLC analysis was 100% methanol. The intensity of the effluent ultraviolet absorbance was monitored at 590 and 468 nm for DAQ and DHQ, respectively. The LC calibration curve was created for quantitative analysis using four standard solutions, that is, 1, 10, 50, and 100 μM (Supplementary Figure S17).

RESULTS AND DISCUSSION

Preparation of Salicylideneanilines-Based Covalent Organic Frameworks. When a triformylphloroglucinol ligand with three –OH groups is used for synthesis of COFs, it produces a mechanically rigid β-ketoenamine-linked COF and no reversible proton tautomerism is observed. This is because the strong intramolecular hydrogen-bonding interactions prevent the reversible proton tautomerism and lock the COFs in the ketoenamine stage.²⁷ To circumvent this, we proposed that the incorporation of the 2,4,6-triformyl phenol moiety with only one –OH group would provide a less rigid β-ketoenamine intermediate and imparts structural flexibility around the pores of the COF needed for undergoing reversible tautomerism.

Phenol, a low-cost and commercially available chemical, was used to synthesize the TFP building block in gram scale with a 56% yield via a Duff reaction.²⁸ SA-COF was prepared by the solvothermal synthesis of a suspension of TFP and TAB in a 5:5:1 (v/v) mixture of 1-butanol, dichlorobenzene, and 6 M aqueous acetic acid (Figure 1). The Fourier transform infrared (FT-IR) spectra of the SA-COF confirm the formation of an imine linkage in the polymers, supported by the disappearance of the N–H stretching signals located at 3450 to 3204 cm⁻¹ and exhibition of the C=N stretching bands located at 1582 cm⁻¹ (Figures 3a and S2). The characteristic resonance peaks of imine carbons at 158.9 and 156.1 ppm were observed in solid-state ¹³C cross-polarization/magic angle spinning nuclear magnetic resonance (CP/MAS NMR) spectra of SA-COF, evidencing the existence of imine linkages (Figure 3e). Thermal gravimetric analyses (TGA) under a N₂ atmosphere show that SA-COF is highly stable up to 500 °C with only 3.8% weight loss (Figure S3). Furthermore, scanning electron microscopy (SEM) and transmission electron microscopy (TEM) reveal that it displays a plait-like morphology and consists of highly crystalline nanoflakes (Figures 2i,j, S5, and S6).

To analyze the crystal structure of the obtained polymer SA-COF, theoretical simulations and powder X-ray diffraction (PXRD) experiments were performed. The calculations were

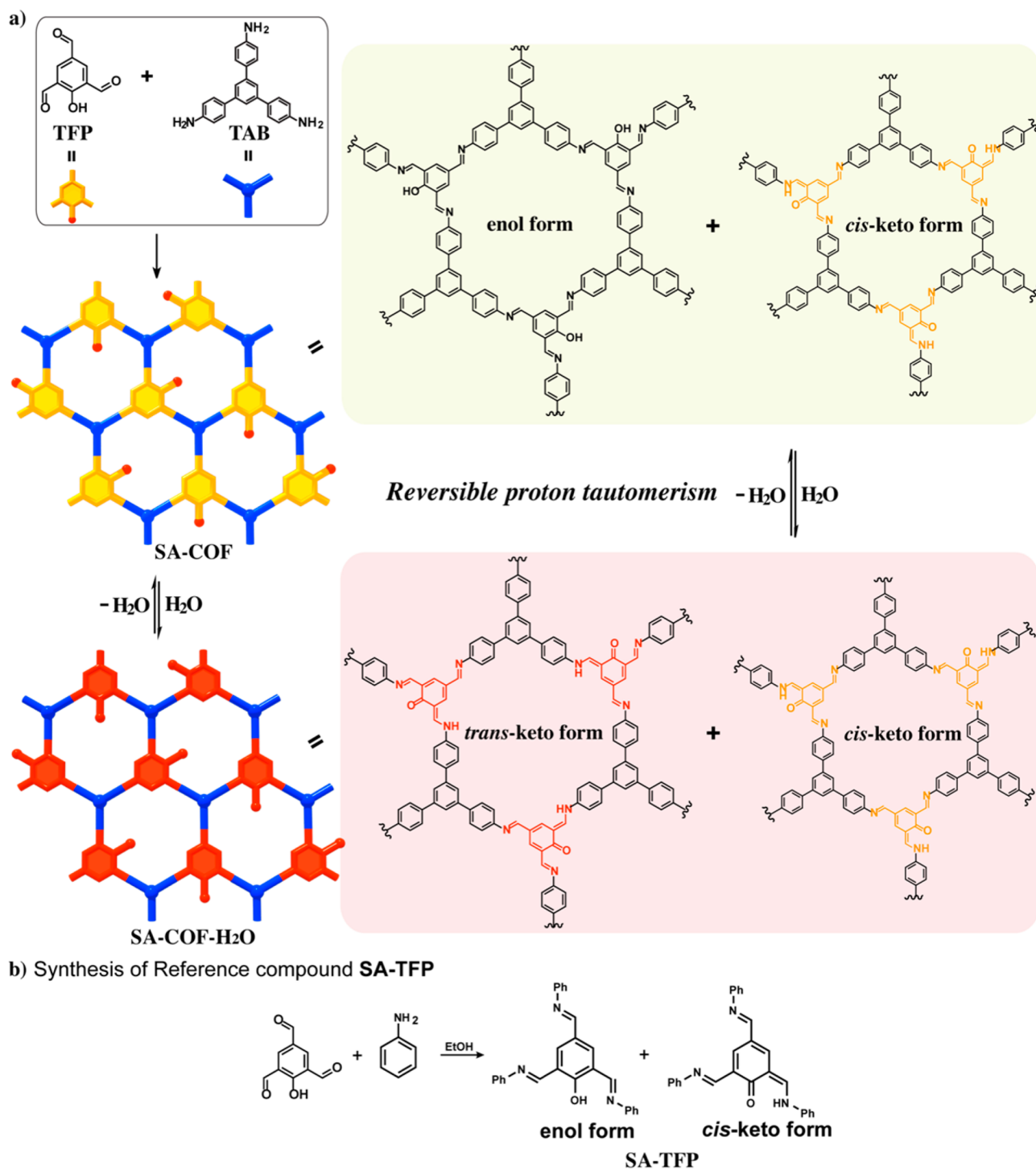


Figure 1. (a) Conceptual representation for synthesis of solvatochromic SA-COF and reversible proton tautomerism triggered by water adsorption and desorption; (b) synthesis of reference compound SA-TFP.

conducted using Material Studio version 2016, and the eclipsed stacking (AA) and staggered stacking (AB) structures were modeled (see Supporting Information for details). In the experimental PXRD pattern of SA-COF (black curve in Figure 2a), an intense peak at 5.68° accompanied by four small peaks at 9.76° , 11.20° , 14.89° , and ca. 25.16° was observed, which can be assigned to (100), (110), (200), (120), and (001) diffractions. The obtained PXRD pattern matches well with the calculated PXRD pattern of the AA stacking structure (Figure 2a,c), suggesting that SA-COF features a highly

uniform pore structure with an AA stacking model. Specifically, Pawley refinement produces a hexagonal space group with unit cell parameters of $a = b = 18.09 \text{ \AA}$, $c = 3.61 \text{ \AA}$, $\alpha = \beta = 90^\circ$, and $\gamma = 120^\circ$, with refinement results of $R_p = 2.91\%$ and $R_{wp} = 4.41\%$. The refined PXRD pattern agrees well with the experimental PXRD data, as confirmed by the vanishing intensity of the difference plot in Figure 2a,b.

The eclipsed AA stacking structure of SA-COF is further supported by the pore size distribution analysis. The nitrogen adsorption–desorption experiment at 77 K (Figure 2g) exhibits

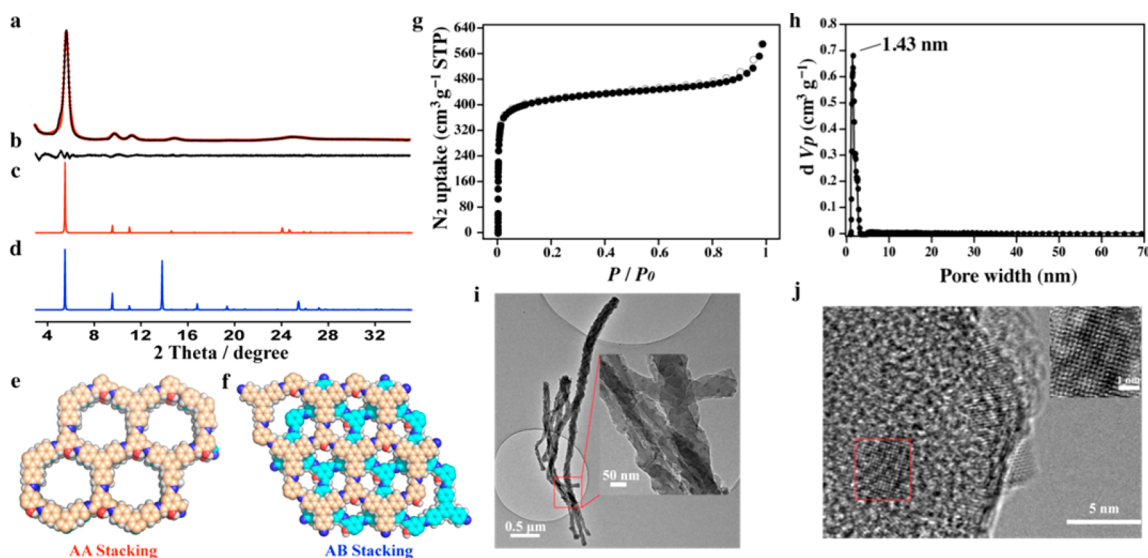


Figure 2. Crystal structure analysis, isotherm profiles of N_2 -gas sorption, and electronic microscope image of SA-COF. (a) Experimental (black line) and refined (red dots) PXRD pattern of SA-COF. (b) Difference curve between experimental and refined PXRD patterns. (c and d) Simulated PXRD pattern of SA-COF with AA (red line) and AB (blue line) stacking structure. (e and f) Top view of the optimized SA-COF in the eclipsed AA stacking and staggered AB stacking mode shown as space-filling model. (g) N_2 adsorption (filled) and desorption (open) isotherm profiles of SA-COF (STP, standard temperature and pressure). (h) Pore-size distribution of SA-COF calculated by nonlocal DFT modeling based on N_2 adsorption data. (i and j) High-resolution TEM image of SA-COF and arrangement of the microspores in the crystalline domain.

a type I N_2 adsorption isotherm that is characteristic of a microporous structure. The Brunauer–Emmett–Teller (BET) surface area of SA-COF is calculated as $1588.56 \text{ m}^2 \text{ g}^{-1}$, and the total pore volume is $0.92 \text{ cm}^3 \text{ g}^{-1}$ ($P/P_0 = 0.99$). The simulated eclipsed-stacked SA-COF structure using nonlocal density functional theory presents a narrow pore size distribution with an average pore width of $\sim 1.43 \text{ nm}$ (Figure 2h), which is very close to the theoretical value of 1.45 nm based on the eclipsed AA stacking structure (Figure 2e).

Proton Tautomerism Triggered by Adsorption and Desorption of Water. When as-synthesized SA-COF powder is exposed to air, its color changes quickly from yellow to deep red (Figure S2), which hints at the existence of proton tautomerism. To investigate the transformation between enol, *cis*-keto, and *trans*-keto forms, UV–vis spectroscopic analysis, FT-IR measurement, and solid-state CP/MAS NMR studies were conducted. In addition, to better understand the proton tautomerization at a molecular level, the molecular reference compound SA-TFP was prepared (Figure 1b), for which the coexistence of enol and *cis*-keto forms in solution and solid-state was confirmed by FT-IR, X-ray, UV–vis, and NMR analysis (Figure 1b and see the Supporting Information for details). UV–vis spectroscopy is a sensitive tool for probing the tautomeric equilibrium in SA compounds. The band below 425 nm can be attributed to the enol form, whereas a contribution peak of the *cis*-keto form appears between 425 and 550 nm , and the signals above 550 nm can be assigned to the *trans*-keto form.^{29,30} The UV–vis spectrum of well-dispersed SA-COF in anhydrous THF was recorded, and it displays two major broadened signals at 300 and 450 nm (Figure S7a), which indicates the coexistence of enol and *cis*-keto forms in the pristine SA-COF at room temperature. In addition, this result is further supported by UV–vis spectra of the reference compound SA-TFP, which shows a similar absorption spectrum (Figure S7b). Without exposure to water molecules, the yellow color of SA-COF originates from the *cis*-keto form. To further elucidate the structure of SA-COF, FT-IR measurements were

conducted. As shown in Figure 3a, the FT-IR spectrum of the pristine sample shows a broad absorption band in the region from 3030 to 2850 cm^{-1} , similar to that in SA-TFP (Figure S2), which indicates the presence of strong resonance-assisted intermolecular hydrogen bonding, reflected by a large-amplitude O–H stretching vibration or proton transfer equilibrium between the O–H enol form and the N–H *cis*-keto form.³¹ In addition, the intense peaks at 1622 and 1503 cm^{-1} originate from C=O and C=C stretching, confirming the existence of the *cis*-keto form. Furthermore, solid-state CP/MAS NMR spectra of SA-COF evidence the proton tautomerism between the enol and *cis*-keto form and agree well with the UV–vis and FT-IR results. Figure 3e shows two very weak characteristic ^{13}C resonances of carbonyl ($^*\text{C}=\text{O}$) and enamine ($^*\text{C}=\text{C}-\text{N}$) carbons at 188.7 and 114.3 ppm , respectively, which are similar to those in the reference compound (190.0 and 115.1 ppm , see Figure S8), confirming the existence of the *cis*-keto form as a minor component. Besides, several characteristic ^{13}C resonances of the enol form including phenol (C1) and imine (C7, C8, and C9) carbons at 162.2 , 158.1 , and 156.1 ppm are observed, which are further supported by comparison with the ^{13}C NMR spectrum of the reference compound SA-TFP (164.3 and 158.4 ppm) (Figures 3 and S8).^{32,33}

When SA-COF is exposed to air, it quickly absorbs water to give red-colored SA-COF- H_2O . The UV–vis spectrum of well-dispersed SA-COF- H_2O in H_2O displays two major broad signals at 430 and 587 nm (Figure S7), indicating the absence of the enol form and the coexistence of the *cis*-keto and *trans*-keto forms in the SA-COF- H_2O . The resulting dark red color of SA-COF- H_2O comes from the *trans*-keto form. In addition, the FT-IR profile of SA-COF- H_2O (Figure 3b) further proves the transformation from enol to keto form by the following changes: (i) the appearance of a large broad stretching peak at $\sim 3420 \text{ cm}^{-1}$ assignable to absorbed H_2O molecules; (ii) the vanishing of the O–H stretching signals located around 2900 cm^{-1} ; (iii) the increment of peak intensity at 1621 cm^{-1}

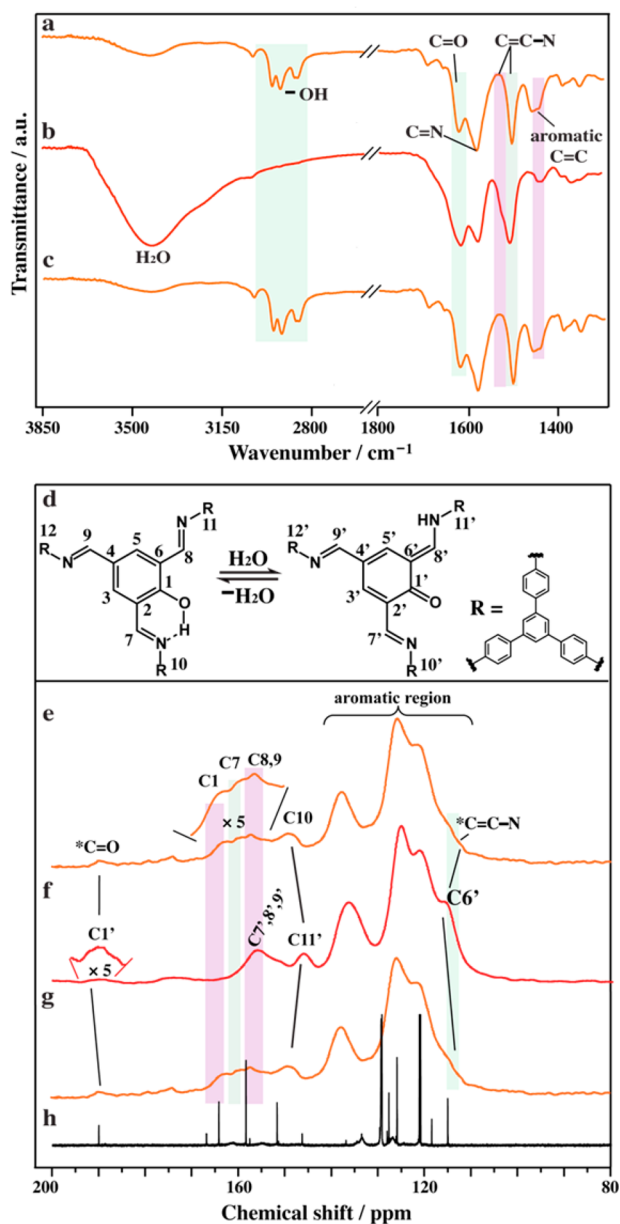


Figure 3. Reversible proton tautomerism evidenced by FT-IR and solid-state CP/MAS NMR. FT-IR spectra of (a) dry SA-COF, (b) SA-COF-H₂O after exposure to air, and (c) SA-COF after desorption of water from SA-COF-H₂O. (d) Schematic presentation of enol and *trans*-keto isomer (the *cis*-keto form is omitted for clarity). Solid-state CP/MAS NMR spectra (100 MHz, 300 K) and assignment of (e) SA-COF; (f) SA-COF-H₂O, and (g) SA-COF produced by desorption of water from SA-COF-H₂O. (h) ¹³C NMR (500 MHz, 300 K, CDCl₃) spectrum of reference compound SA-TFP, exhibiting the coexistence of the enol and *cis*-keto forms. (*C=O and *C=C-N represent the carbonyl and enamine carbons in the *cis*-keto form, respectively.)

attributed to C=O stretching; (iv) the decrease of signal intensity at 1582 cm⁻¹ assigned to C=N stretching; (v) the appearance of a new peak at 1531 cm⁻¹ corresponding to C=C stretching in *trans*- β -ketoenamine, and (vi) the decline of peak intensity at 1450 cm⁻¹ assignable to the aromatic C=C stretching. More importantly, the solid-state CP/MAS NMR spectrum of SA-COF-H₂O (Figure 3f) also supports such transformation by the following evidence: (i) the increment of signal intensity of the carbonyl carbon (C1') at 190.7 ppm

corresponding to the increment of *trans*-keto population; (ii) the low-field shift of the *cis*-keto at 188.7 ppm to 190.7 ppm attributed to breaking of the intramolecular hydrogen bonding; (iii) the disappearance of C1 and C7 resonances in the enol form; (iv) the rise of peak intensity at 116.3 ppm attributed to C6' resonances in the *trans*-keto form. Interestingly, when SA-COF-H₂O is heated at 120 °C under vacuum, adsorbed water molecules are removed, and it returns back to the original yellow colored SA-COF with identical UV-vis, FT-IR, and solid-state CP/MAS NMR spectra (Figure 3c,g). All these data clearly demonstrate reversible proton tautomerism between the enol and *cis*- and *trans*-keto in SA-COF, which is readily triggered by the adsorption and desorption of water molecules (see the proposed mechanism of proton tautomerism in the Supporting Information).

Size-Dependent Separation. The removal of water-soluble organic pollutants by a porous material is an important research field due to rising environmental problems.^{34–36} The tunable functionality of the pore surface in SA-COF induced by proton tautomerism can be exploited for the separation of molecules based on size, charge, and functionality. To demonstrate size-selective adsorption, we have chosen several water-soluble dye molecules (Figure 4), specifically MB, RB, and CA. As shown in Figure 4, the van der Waals sizes of these molecules are calculated using Material Studio 2016. The size of these dye molecules follows the order MB < RB \lesssim pore size of SA-COF < CA. Ultraviolet-visible (UV-vis) spectroscopy was used to monitor the change of concentration of dye in a fixed time interval. SA-COF has the ability to quickly adsorb and remove organic dye (MB) from water (Figure 5a). The size exclusion effect of SA-COF was tested by selecting three molecules with different sizes, and we found that the binding affinity of SA-COF for dye molecules declines with an increase in molecular size. As shown in Figures 5b and S13, the smallest size dye, MB, was completely removed within 10 min, showing a removal efficiency of 98.3%, while the larger size RB, which is slightly smaller than the pore size of SA-COF, exhibits a much slower adsorption rate (~60 min) and with 94.1% removal efficiency compared to that of MB. The largest dye, CA, whose size is larger than 1.45 nm, exhibits no noticeable change of its concentration during the adsorption tests. Meanwhile, when the dyes MB and CA were treated with commercial porous activated carbon, they did not show good separation performance (see Figure S16). The size-dependent adsorption reflects the highly uniform pore size distribution of SA-COF (~1.43 nm), rendering it a useful molecular sieve material based on size exclusion. To test this, SA-COF powder was suspended and stirred in a green-colored aqueous solution of MB and CA (1:1 molar ratio) for 10 min at rt. After filtration, the UV-vis spectra before and after SA-COF treatment show that the MB and CA mixture can be completely separated and the concentration of MB is decreased by 99.9%, while CA does not show any notable change (Figure 5d). It should be stated here that the size of the dye molecule may not be the only factor at play; charge and functional groups in the dye molecules may act in concert with its size to effect size-dependent adsorption in the SA-COF.

Charge-Selective Separation. Since the -OH and -NH moieties in SA-COF can be deprotonated or protonated in basic or acidic conditions, respectively, SA-COF is expected to be a promising platform for separation of charged molecules due to its pH-controllable ionicity. Before the separation test, the stability of SA-COF in base (pH = 12, 0.01 M NaOH) or

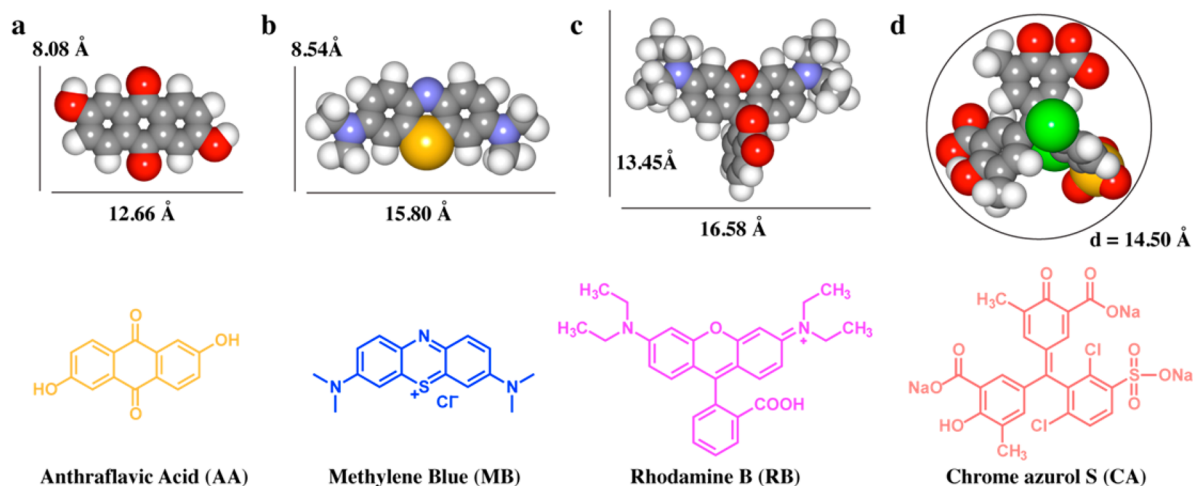


Figure 4. Dye molecules used in molecular separation experiments based on size and charge. Molecular model (top) calculated from Material Studio 2016, displayed in space-filling style (gray, carbon; red, oxygen; white, hydrogen; blue, nitrogen; green, chlorine; yellow, sulfur) and chemical structure of dye molecules (bottom); (a) anthraflavic acid with a size of 8.08 × 12.66 Å, (b) methylene blue with a size of 8.54 × 15.80 Å, (c) rhodamine B with a size of 13.45 × 16.58 Å, (d) Chrome azurol S with a diameter of 14.50 Å.

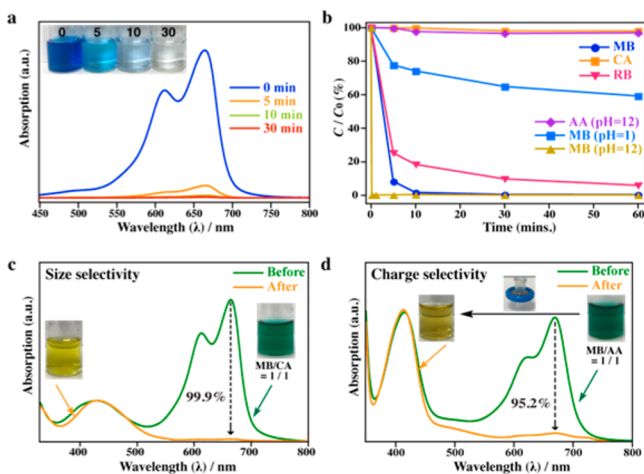


Figure 5. Size- and charge-selective separation experiments. (a) UV-vis absorption spectra of an aqueous solution of MB after treatment with SA-COF at different intervals. (b) Change in concentration of dye over time after treatment with SA-COF, determined by change in absorbance relative to initial absorbance (C/C_0). The data are averaged over three test trials. (c) UV-vis absorption spectra of size-selective separation of CA from a mixture of CA and MB in water (green and orange lines represent before and after treatment with SA-COF, respectively; inset, photographs of CA and MB mixture and filtrate after treatment with SA-COF, showing green and deep yellow color). (d) UV-vis absorption spectra of charge-selective separation of AA from a mixture of AA and MB in water (green and orange lines represent before and after treatment with SA-COF, respectively; inset, photo image of green-colored CA and MB mixture, deep yellow colored filtrate after passing through the filter disc charged with SA-COF powders).

acid (pH = 1, 0.1 M HCl) was examined. SA-COF retained its original crystalline structure in base or acid, as indicated by the unchanged intensities and positions of the peaks in its PXRD profile (Figure S12). SA-COF powder was added to an aqueous solution of AA (Figure 4a), a negatively charged dye at basic conditions (pH = 12), and no remarkable change in the concentration of AA was found, as confirmed by UV-vis spectroscopy (Figures 5b and S14). In contrast, MB, which has a similar size to AA but positively charged instead, was rapidly

absorbed within 10 s (99.8% removal efficiency) in the same conditions (Figure 5b), showing a large increment of uptake rate compared to the neutral SA-COF (98.3% removal efficiency at 10 min), suggesting that electrostatic attraction is operational here. However, when the dyes AA and MB were treated with commercial porous activated carbon in the same conditions, they did not show any selective separation (see Figure S16). To further test the charge separation effect, a green-colored AA and MB mixture in 1:1 ratio was quickly passed through (~10 s) a filter in which the base-treated SA-COF powders were pre-equipped (for details see the Experimental Section). The UV-vis spectra before and after filter treatment revealed that the AA and MB mixture was clearly separated, and there was a sharp decrease in MB concentration (95.2%) (Figure 5d); however, almost no change was observed for the concentration of AA. More interestingly, the absorption ability of SA-COF toward MB can be reversed. When the SA-COF powder was added into an acidic aqueous solution of MB, the concentration of MB showed a much slower decrease with 22% removal efficiency within 5 min than that in basic conditions (99.8% removal efficiency at 10 s) (Figures 5b and S14).

Chemoselective Separation. Owing to the basic N-H moiety in the *trans*-keto form, SA-COF can discriminate functional groups with different acidity, and it selectively binds -OH over -NH₂ groups under neutral conditions. Two molecules of the same size, but with different functional groups, 1,4-dihydroxyanthraquinone and 1,4-diaminoanthraquinone, are chosen as model compounds (Figure 6a). SA-COF powder was added to a solution of DHQ in an ethanol and water mixed solvent ($V_{\text{EtOH}}/V_{\text{H}_2\text{O}} = 2/3$), and a significant decrease in concentration of DHQ with almost 90% removal efficiency within 60 min was observed by UV-vis spectroscopy. In contrast, the concentration of DAQ was only slightly decreased with ~25% removal efficiency within 60 min, resulting in a high selectivity with a ratio of 1:7 of DHQ:DAQ in the filtrate (Figures 6a and S15). The molecular selectivity is further demonstrated in a separation experiment: when a 1:1 mixture of DHQ and DAQ was treated with SA-COF powder, within 10 min, the ratio of DHQ:DAQ was found to be 1:6 in the filtrate, as confirmed by HPLC analysis (Figure 6b).

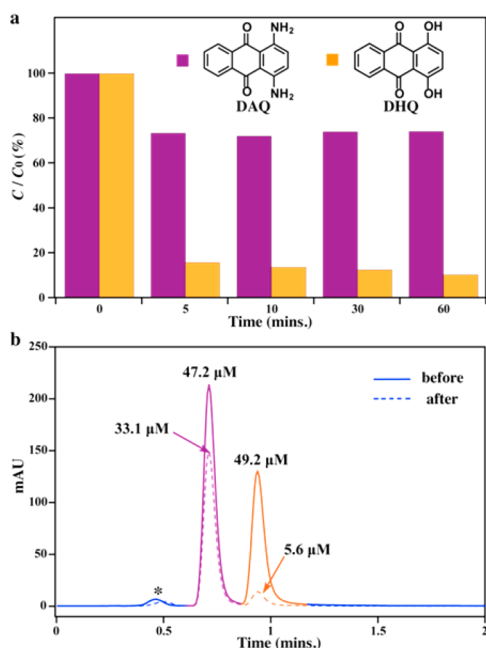


Figure 6. Chemoslective separation experiments. (a) UV–visible absorbance spectra of DAQ and DHQ at different time intervals after treatment with SA-COF (purple, DAQ; orange, DHQ). The data are averages of triplicate experiments. (b) HPLC spectra of a DAQ and DHQ mixture in 1:1 molar ratio before and after treatment with SA-COF (full line: before; dotted line: after; purple (DAQ) and orange (DHQ) peaks with 0.693 and 0.914 min retention times, respectively; * marks the solvent peak).

CONCLUSION

We have successfully synthesized salicylideneanilines-based COF, which exhibits reversible solvatochromism triggered by adsorption and desorption of water molecules. Our studies show that inborn, chemoresponsive pores can be programmed into COF by reticular synthesis. The reversible proton tautomerism was confirmed by UV–vis spectroscopy, FT-IR, and solid-state CP/MAS NMR analysis. The tautomerization of SA-COF stimulates dynamic changes in the ionic and chemical properties of the pores and allows molecular separation on the basis of size exclusion, charge separation, and functional group discrimination. Specifically, it binds positively charged molecules in basic conditions, while excluding them in acidic conditions. Moreover, SA-COF can discriminate functional groups with different degrees of acidity; that is, it prefers to bind to molecules with aromatic hydroxyl groups rather than aromatic amino groups. Our studies open an avenue for designing smart, chemoresponsive COFs, further attesting to the utility of COFs as flexible and tunable materials for molecular separation applications.

ASSOCIATED CONTENT

Supporting Information

The Supporting Information is available free of charge on the ACS Publications website at DOI: 10.1021/jacs.7b02696.

Additional experimental procedures and structural modeling, IR, TGA, BET analysis, SEM and TEM images, UV–vis spectrum, solid-state CP/MAS NMR spectra, the proposed mechanism of proton tautomerism, selectivity experiment, control experiment, and HPLC analysis (PDF)

AUTHOR INFORMATION

Corresponding Author

*chmlhkp@nus.edu.sg

ORCID

Guo-Hong Ning: 0000-0002-5640-9062

Kian Ping Loh: 0000-0002-1491-743X

Notes

The authors declare no competing financial interest.

ACKNOWLEDGMENTS

K.P.L. acknowledges NRF-CRP grant “Two Dimensional Covalent Organic Framework: Synthesis and Applications”, grant number NRF-CRP16-2015-02, funded by National Research Foundation, Prime Minister’s Office, Singapore.

REFERENCES

- (1) Adrien, P.; Côté, A. P.; Benin, A. I.; Ockwig, N. W.; O’Keeffe, M.; Matzger, A. J.; Yaghi, O. M. *Science* **2005**, *310*, 1166–1170.
- (2) Waller, P. J.; Gándara, F.; Yaghi, O. M. *Acc. Chem. Res.* **2015**, *48*, 3053–3063.
- (3) Feng, X.; Ding, X.; Jiang, D. *Chem. Soc. Rev.* **2012**, *41*, 6010–6022.
- (4) Ding, S. Y.; Wang, W. *Chem. Soc. Rev.* **2013**, *42*, 548–568.
- (5) Slater, A. G.; Cooper, A. I. *Science* **2015**, *348*, aaa8075.
- (6) Doonan, C. J.; Tranchemontagne, D. J.; Glover, T. G.; Hunt, J. R.; Yaghi, O. M. *Nat. Chem.* **2010**, *2*, 235–238.
- (7) Huang, N.; Krishna, R.; Jiang, D. *J. Am. Chem. Soc.* **2015**, *37*, 7079–7082.
- (8) DeBlase, C. R.; Silberstein, K. E.; Truong, T.-T.; Abruña, H. D.; Dichtel, W. R. *J. Am. Chem. Soc.* **2015**, *135*, 16821–16824.
- (9) Xu, F.; Jin, S.; Zhong, H.; Wu, D.; Yang, X.; Chen, X.; Wei, H.; Fu, R.; Jiang, D. *Sci. Rep.* **2015**, *5*, 8225.
- (10) Liu, W.; Luo, X.; Bao, Y.; Liu, Y. P.; Ning, G.-H.; Abdelwahab, I.; Li, L.; Nai, C. T.; Hu, Z. G.; Zhao, D.; Liu, B.; Quek, S. Y.; Loh, K. P. *Nat. Chem.* **2017**, *9*, 563–570.
- (11) (a) Fang, Q.; Wang, J.; Gu, S.; Kaspar, R. B.; Zhuang, Z.; Zheng, J.; Guo, H.; Qiu, S.; Yan, Y. *J. Am. Chem. Soc.* **2015**, *137*, 8352–8355. (b) Fang, Q.; Zhuang, Z.; Gu, S.; Kaspar, R. B.; Zheng, J.; Wang, J.; Qiu, S.; Yan, Y. *Nat. Commun.* **2014**, *5*, 4503.
- (12) Ding, S.-Y.; Gao, J.; Wang, Q.; Zhang, Y.; Song, W.-G.; Su, C.-Y.; Wang, W. *J. Am. Chem. Soc.* **2011**, *133*, 19816–19822.
- (13) Lin, S.; Diercks, C. S.; Zhang, Y.-B.; Kornienko, N.; Nichols, E. M.; Zhao, Y.; Paris, A. R.; Kim, D.; Yang, P.; Yaghi, O. M.; Chang, C. J. *Science* **2015**, *349*, 1208–1213.
- (14) Xu, H.; Gao, J.; Jiang, D. *Nat. Chem.* **2015**, *7*, 905–912.
- (15) Ding, X.; Guo, J.; Feng, X.; Honsho, Y.; Guo, J.; Seki, S.; Maitarad, P.; Saeki, A.; Nagase, S.; Jiang, D. *Angew. Chem., Int. Ed.* **2011**, *50*, 1289–1293.
- (16) Guo, J.; Xu, Y.; Jin, S.; Chen, L.; Kaji, T.; Honsho, Y.; Addicoat, M. A.; Kim, J.; Saeki, A.; Ihee, H.; Seki, S.; Irlé, S.; Hiramoto, M.; Gao, J.; Jiang, D. *Nat. Commun.* **2013**, *4*, 2736.
- (17) Xu, H.; Tao, S.; Jiang, D. *Nat. Mater.* **2016**, *15*, 722–726.
- (18) Ding, S.-Y.; Dong, M.; Wang, Y.-W.; Chen, Y.-T.; Wang, H.-Z.; Su, C.-Y.; Wang, W. *J. Am. Chem. Soc.* **2016**, *138*, 3031–3037.
- (19) Cohen, M. D.; Schmidt, G. M. J.; Flavian, S. *J. Chem. Soc.* **1964**, 2041–2051.
- (20) Hadjoudis, E.; Vittorakis, M.; Mavridis, I. M. *Tetrahedron* **1987**, *43*, 1345–1360.
- (21) Amimoto, K.; Kawato, T. *J. Photochem. Photobiol., C* **2005**, *6*, 207–226.
- (22) Hadjoudis, E.; Mavridis, I. M. *Chem. Soc. Rev.* **2004**, *33*, 579–588.
- (23) Cohen, M. D.; Flavian, S.; Leiserowitz, L. *J. Chem. Soc. B* **1967**, 329–334.
- (24) Ogawa, K.; Kasahara, Y.; Ohtani, Y.; Harada, J. *J. Am. Chem. Soc.* **1998**, *120*, 7107–7108.

- (25) Harada, J.; Uekusa, H.; Ohashi, Y. *J. Am. Chem. Soc.* **1999**, *121*, 5809–5810.
- (26) (a) Gao, Q.; Bai, L.; Zeng, Y.; Wang, P.; Zhang, X.; Zou, R.; Zhao, Y. *Chem. - Eur. J.* **2015**, *21*, 16818–16822. (b) Gao, Q.; Bai, L.; Zhang, X.; Wang, P.; Li, P.; Zeng, Y.; Zou, R.; Zhao, Y. *Chin. J. Chem.* **2015**, *33*, 90–94.
- (27) Kandambeth, S.; Mallick, A.; Lukose, B.; Mane, M. V.; Heine, T.; Banerjee, R. *J. Am. Chem. Soc.* **2012**, *134*, 19524–19527.
- (28) Anderson, A. A.; Goetzen, T.; Shackelford, S. A.; Tsank, S. *Synth. Commun.* **2007**, *30*, 3227–3232.
- (29) Fujiwara, T.; Harada, J.; Ogawa, K. *J. Phys. Chem. B* **2004**, *108*, 4035–4038.
- (30) Jacquemin, P.-L.; Robeyns, K.; Devillers, M.; Garcia, Y. *Chem. - Eur. J.* **2015**, *21*, 6832–6845.
- (31) Ambroziaka, K.; Rozwadowska, Z.; Dziembowska, T.; Biegb, B. *J. Mol. Struct.* **2002**, *615*, 109–120.
- (32) Schilfa, W.; Kamińska, B.; Kołodziej, B.; Grechb, E.; Rozwadowska, Z.; Dziembowska, T. *J. Mol. Struct.* **2002**, *615*, 141–146.
- (33) Claramunt, R. M.; López, C.; María, M. D. S.; Sanz, D.; Elguero, J. *Prog. Nucl. Magn. Reson. Spectrosc.* **2006**, *49*, 169–206.
- (34) Schwarzenbach, R. P.; Escher, B. I.; Fenner, K.; Hofstetter, T. B.; Johnson, C. A.; Gunten, U.; Wehrli, B. *Science* **2006**, *313*, 1072–1077.
- (35) Alsbauer, A.; Smith, B. J.; Xiao, L.; Ling, Y.; Helbling, D. E.; Dichtel, W. R. *Nature* **2016**, *529*, 190–194.
- (36) Byun, J.; Patel, H. A.; Thirion, D.; Yavuz, C. T. *Nat. Commun.* **2016**, *7*, 13377.